Development of a Variable-Reluctance Spherical Motor

Kok-Meng Lee, Xiao-an Wang
George W. Woodruff School of Mechanical Engineering
Georgia Institute of Technology

Abstract

This paper presents the dynamic modeling and the control strategy of an interesting three degrees-of-freedom (DOF) variable-reluctance (VR) spherical motor which presents some attractive possibilities by combining pitch, roll, and yaw motion in a single joint. Both the forward dynamics which determine the motion as a result of activating the electromagnetic coils and the inverse model which determines the coil excitations required to generate the desired torque are derived. The solution to the forward dynamics of the spherical motor is unique but the inverse model has multiple solutions and therefore an optimal choice is required. The implementation issues in determining the optimal control input vectors in real-time are also addressed.

1. INTRODUCTION

An increasing need for high performance robotic applications has motivated several researchers to investigate new actuator concepts for improving the dexterity of robotic wrists. Examination of the existing mechanical joints reveals that the ball-joint-like spherical actuator is an attractive alternative to the three consecutive-rotational joint configuration. The interest in spherical motor as a robot wrist is triggered because of its ability in providing the roll, yaw, and pitch motion in a single joint, isotropic in kinematics and kinetics, and its relatively simple structure. Also, it has no singularity in the middle of workspace except at the boundary. The elimination of gears and linkages enables both high positioning precision and fast dynamic response to be achieved by a properly designed spherical motor. These attractive features have potential applications such as high-speed plasma and laser cutting where the orientation must be achieved rapidly and continuously in all directions.

Recently, several design concepts of spherical motor were proposed. A spherical induction motor was conceptualized in [1] for robotic applications and the detailed analysis was given in [2]. However, it is difficult to realize a prototype of its kind because of its complexity in mechanical and winding design and manufacturing, which requires inlaying all three transversing windings on the inner spherical surface of the stator. Laminations are required to prevent movement of unwanted eddy currents. Complicated three phase windings must be mounted in recessed grooves in addition to the rolling supports for the rotor in a static configuration. These and other considerations have led Lee et al. [3] to investigate an alternative spherical actuator based on the concept of VR stepper motor which is easier to manufacture. Hollis et al. [4] has developed a six DOF direct-current (DC) "magic wrist" as part of a coarse-fine robotic manipulator. An alternative DC spherical motor design with three DOF in rotation was demonstrated by Kanedo et al. [5], which can spin continuously and has a maximum inclination of 15°. Although the control of a DC spherical motor is relatively simple, the range of inclination and the torque constant are rather limited. Foggia et al. [6] demonstrated an induction type spherical motor of different structure, which has a range of motion characterized by a cone of 60°. Since the control strategy of the induction motor [6] has not been reported, no results were given on the ability of the motor to realize any arbitrary motions.

As compared with its DC counterpart, a VR spherical motor has a relatively large range of motion, possesses isotropic properties in motion, and is relatively simple and compact in design. The trade-off, however, is that sophisticated control scheme is required. For this reason, in this paper we discuss both the dynamic model and the control strategy of a VR spherical motor. For motion control of the VR spherical motor, both the forward dynamics which determine the motion as a result of activating the motor coils and the inverse model which determines the coil excitations required to obtain the desired torques are needed. The solution to the forward dynamics of the spherical motor is unique but the inverse model, however, has multiple solutions and therefore an optimal choice is required.

The remaining paper is organized as follows: Section 2 begins with the derivation of the torque prediction equations. Section 3 presents the motion control strategy of the spherical motor, which consists of the control of the rotor dynamics and the determination of the optimal input vector. The real-time implementation of the optimization method is addressed in Section 4. The conclusions are given in Section 5.

2. DYNAMIC MODEL

The VR spherical motor referred to in this paper is a ball-joint-like device similar to that conceptualized by Lee and Kwan [7].

2.1 Description of a VR Spherical Motor

The VR spherical motor is shown in Fig. 1 and an exploded graphical view is given in Fig. 2. The VR spherical motor consists of basically three mechanical assemblies; namely, a spherical rotor, a hollow spherical stator, and a orientation measuring system. The spherical rotor is constrained but allows to roll on the bearing gimbals which are mounted on the inner surface of the stator.

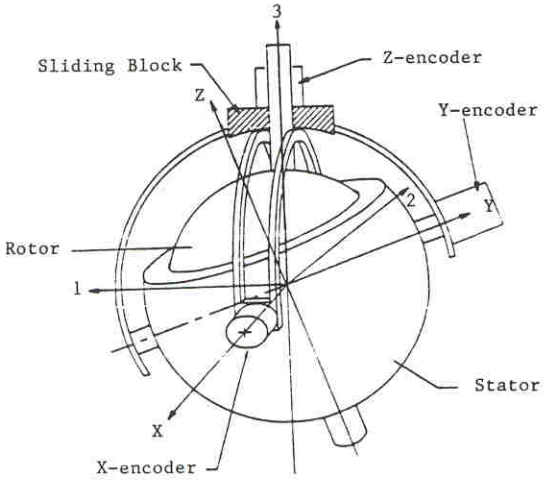

Fig. 1 Structure of a VR Spherical Motor

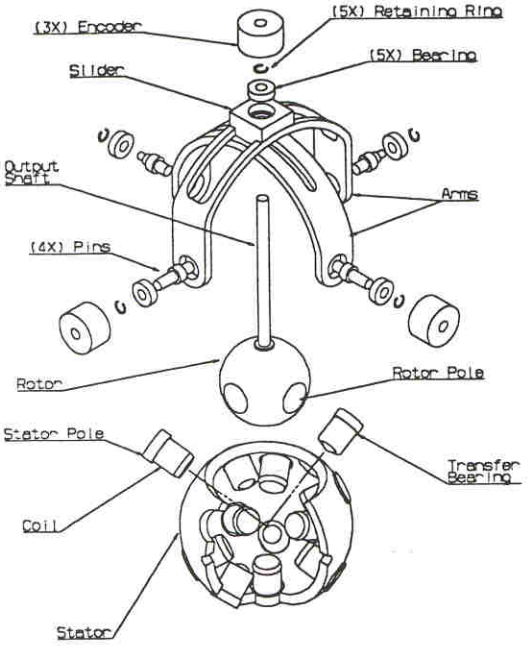

Fig. 2 Assembly View of a VR Spherical Motor

The coils with ferromagnetic cores are evenly located on the rotor and the stator, and each coil can be energized individually. In order to maintain geometrical symmetry for simplicity in control, the stator and the rotor poles are of circular shape and are evenly spaced on the stator and the rotor following the pattern of regular polyhedrons. Each vertex of the polyhedron corresponds to the location of one pole. Pythagoras and Plato [8] have shown that a complex polyhedral angle must be made up of at least three faces and must be less than 360° to form a closed polyhedron. Using these principles, it can be shown that the maximum number of coils which can be evenly spaced on a sphere is 20, the figure corresponding to the number of complex angles of a dodecahedron. The influences of the design configuration on motion feasibility and the methodology of selecting the patterns has been discussed in reference [9].

The rotor poles meet at the center of the rotor, and the stator cores are connected by the magnetic conductor layer in the stator shell to form a magnetic circuit with the airgap. In the operation of the VR spherical motor, the stator coils are energized individually using the control circuitry. A magnetic field is established which creates magnetic energy in the airgap. The created energy is the function of the relative position of the rotor and the stator. The motion of the VR spherical motor is thus generated as the rotor tends to move to a position such that the energy in the airgap is minimized.

The measurement mechanism consists of two circular sliding guides mounted on two orthogonal axles attached to the stator. The sliding guides confine a sliding block which houses an encoder for measuring the spin angle of the rotor, θ_z. When the rotor shaft rotates relative to the stator, the corresponding angles rotated by the x- and y- sliding guides are measured by the encoders as θ_x and θ_y. The detailed kinematic relationship which describes the orientation of the rotor as a function of the three encoder readings has been given in reference [9].

2.2 Rotor Dynamics

A base Cartesian coordinate frame XYZ is fixed at the center of the spherical stator with the X and Y axes pointing towards the x- and y- encoders and the Z axis pointing toward the open-end of the spherical socket. Similarly, a coordinate frame 123 is assigned to the center of the spherical rotor with the 3 axis pointing along the rotor shaft. As it will be discussed later, the structure of the spherical motor has certain symmetric properties with respect to Z-Y-Z Euler angles, which are greatly exploited in solving the optimal control input for a specified torque. Thus, the orientation of the spherical motor is specified using the Z-Y-Z Euler angles. Given an actuating torque $\mathbf{T} = [T_1, T_2, T_3]^T$, the rotor dynamic equations described in terms of Z-Y-Z Euler angles $\mathbf{q} = [\psi, \theta, \phi]^T$ is given as follows:

$$\mathbf{M(q)}\,\ddot{\mathbf{q}} + \mathbf{h(q, \dot{q})} = \mathbf{T}, \qquad (1)$$

where $\mathbf{M(q)}$ is the 3x3 inertia matrix of the rotor; $\mathbf{h(q, \dot{q})}$ is a 3x1 vector of centrifugal and Coriolis terms; and T is the actuating torque of the motor.

The actuating torque of the spherical motor is derived by using a linearized model based on a lumped-parameter approach. The linearized model allows the flux flowing through the reluctance of airgaps to be considered separately, and yet permits a wide variety of coil excitations to be analyzed.

Electro-magnetic system

In the derivation of the analytical model, the reluctance of the iron core is assumed to be negligible as compared to that of the airgap and thus the energy storage occurs solely in the air gap. The error introduced by this assumption depends on the geometrical dimensions of the structure and the permeability. This error, in general, can be significantly reduced with magnetic materials of high permeability and with small airgap. The spacing between any adjacent rotor poles and that between any adjacent stator poles is assumed to be much larger compared to the airgap. This

assumption implies that no leakage flux occurs between adjacent stator (or rotor) poles.

The electro-magnetic system of the VR spherical motor is modelled as shown in Fig. 3 for the derivation of the torque generation. The VR spherical motor consists of m active stator coils and n active rotor coils. In Fig. 3, M_{si} and M_{rj} denote the magneto-motive-forces (mmf's), which are the electrical inputs to the i^{th} stator coil and the j^{th} rotor coil respectively; R_{ij} denotes the reluctance of the airgap between the i^{th} stator coil and the j^{th} rotor coil; and Φ_{ij} is the corresponding flux flowing through R_{ij}. The magnetic potential at the stator shell with respect to that of the center of the rotor is denoted as V in Fig. 3.

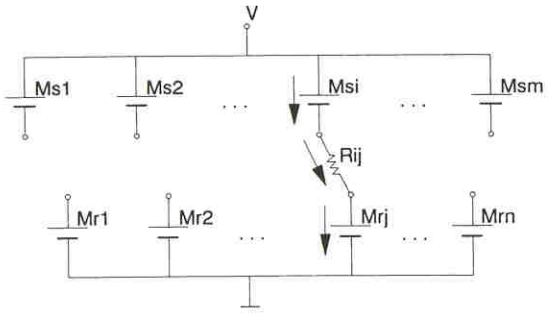

Fig. 3 Magnetic Circuit of the Spherical VR Motor

With the aid of Fig. 3, the magnetic flux Φ_{ij} can be determined from Equation (2).

$$\Phi_{ij} = P_{ij} [M_{si} + M_{rj} - V] \tag{2}$$

where the permeance P_{ij} is the reciprocal of R_{ij}. Since

$$\sum_{i=1}^{m} \sum_{j=1}^{n} \Phi_{ij} = 0, \tag{3}$$

the magnetic potential V can be derived by substituting Φ_{ij} from Equation (2) into Equation (3), which leads to

$$V = \frac{\sum_{i=1}^{m} \sum_{j=1}^{n} P_{ij} (M_{si} + M_{rj})}{\sum_{i=1}^{m} \sum_{j=1}^{n} P_{ij}} \tag{4}$$

Governing equations of energy conversion

The torque generated by the electro-magnetic system is derived by using the principle of conservation of energy:

$$\dot{E}_m(t) = \dot{E}_e(t) - \mathbf{T}(t) \bullet \omega(t) \tag{5}$$

where

$\dot{E}_m$ = time rate of magnetic energy stored,

$\dot{E}_e$ = electrical power input,

$\mathbf{T}$ = resultant torque acting on the rotor, and

ω = angular velocity of the rotor.

Since

$$\mathbf{T} \bullet \omega \, dt = T_x d\phi_x + T_y d\phi_y + T_z d\phi_z , \tag{6}$$

where $d\phi_x$, $d\phi_y$ and $d\phi_z$ are the infinitesimal changes of angles with respect to the stator frame. Using the result from Equations (5) and (6) and noting that the differentials of ϕ_x, ϕ_y, and ϕ_z are independent of each other, the torque generated by the magnetic system is given by

$$\mathbf{T} = \nabla (E_e - E_m) , \tag{7}$$

where

$$\nabla = \left(\frac{\partial}{\partial \phi_x}\right) \mathbf{i} + \left(\frac{\partial}{\partial \phi_y}\right) \mathbf{j} + \left(\frac{\partial}{\partial \phi_z}\right) \mathbf{k}$$

and **i, j, k** are the unit vectors along the X, Y, Z axes of the stator coordinate respectively. The electrical power input to the system is given by

$$\dot{E}_e = \sum_{i=1}^{m} \sum_{j=1}^{n} (M_{si} + M_{rj}) \dot{\Phi}_{ij} \tag{8}$$

and the total magnetic energy stored in the system is

$$E_m = \frac{1}{2} \sum_{i=1}^{m} \sum_{j=1}^{n} \Phi_{ij}^2 R_{ij} \tag{9}$$

From Equation (8) and the time-derivative of E_m obtained from Equation (9):

$$\dot{E}_e - \dot{E}_m = \frac{1}{2} \sum_{i=1}^{m} \sum_{j=1}^{n} (M_{si} + M_{rj} - V)^2 \dot{P}_{ij} . \tag{10}$$

Thus, the torque can be derived by Equation (11) by combining Equations (1), (6), and (10) and noting that ϕ_x, ϕ_y and ϕ_z are independent:

$$\mathbf{T} = \frac{1}{2} \sum_{i=1}^{m} \sum_{j=1}^{n} (M_{si} + M_{rj} - V)^2 \nabla P_{ij} \tag{11}$$

2.3 Permeance Function

Both numerical computation [10] and experimental results [7] have indicated that a typical permeance model P(x), where x is the relative displacement between two poles, has the following properties:

1. P(x) is even, positive, and monotonically decreasing to zero as the displacement increases.
2. The derivative of P(x) has a local maximum or minimum at $x = \pm x_m$, where x_m is a constant for a given geometry.
3. The value of P(x) at the origin (i.e. when the poles are fully overlapped) can be determined by

$$P(x) = \frac{\mu_o S(x)}{\ell} \tag{12}$$

where μ_o is the permeanability of air; ℓ is the shortest path length between two parallel pole-faces; and S(x) is the overlapping area between the stator pole and the rotor pole. For a given geometry, a typical permeance curve which satisfies the above conditions is given as follows:

$$\frac{P(x)}{P(x=0)} = \frac{1}{1 + \chi^2} \tag{13}$$

where $\chi = x/x_o$, where x_o is a constant to be determined. By noting that the corresponding maximum permeance occurs at $x_m = x_o/\sqrt{3}$, the value of x_o can be determined experimentally or from numerical computation such as using finite element method. However, the following additional condition must be satisfied in modeling the permeance function for the spherical motor: P(x) must be periodic with a period 2π. Thus, using Fourier series expansion on $[-\pi, \pi]$ and retain the first N terms, the following periodic permeance function can be obtained.

$$P(x) = a_o + \sum_{k=1}^{N} a_k \cos k x \tag{14}$$

where the coefficients (a_0, a_1, ..., a_N) can be determined from experimental data or from numerical computation. Note that P(x) is an even function and therefore the sine terms vanish.

2.4 Torque Prediction Model

The torque prediction model determines the torque generated by the spherical motor for a given set of input currents applied to the electromagnetic coils. For a specified geometry, the permeance between any pairs of adjacent stator and rotor poles is a function of the angle between the position vectors characterizing of i^{th} stator and the j^{th} rotor poles, ϕ_{ij}. Let

$$P_{ij} = P(\phi_{ij}). \tag{15}$$

Let $\mathbf{C_{si}}(x_{si}, y_{si}, z_{si})$ and $\mathbf{C_{rj}}(x_{rj}, y_{rj}, z_{rj})$ be the position vectors of the i^{th} stator and the j^{th} rotor poles respectively. The angle between any pairs of stator and rotor poles can be determined from the dot inner product of the position vectors $\mathbf{C_{si}}$ and $\mathbf{C_{rj}}$; that is

$$\cos(\phi_{ij}) = \frac{\mathbf{C_{si}} \bullet \mathbf{C_{rj}}}{R^2} \tag{16}$$

where R is the mean radius of a spherical surface separating the pole faces of the stator and rotor. The position vector of the j^{th} rotor coil with respect to the stator coordinate frame is defined by

$$\begin{bmatrix} C_{rj} \\ 1 \end{bmatrix}_{XYZ} = [T] \begin{bmatrix} c_{rj} \\ 1 \end{bmatrix}_{123}, \tag{17}$$

where [T] is a homogeneous transformation describing the rotor frame with respect to stator frame, and $\mathbf{c_{rj}}$ describe the position vectors of j^{th} rotor pole with respect to the rotor frame. From Equations (7) and (11), it can be shown by using differential geometry that the torque is given by

$$\mathbf{T} = \frac{1}{2} \sum_{i=1}^{m} \sum_{j=1}^{n} [(M_{si} + M_{rj} - V)^2 \bullet \left.\frac{dP(\phi)}{d\phi}\right|_{\phi=\phi_{ij}} \mathbf{e_{ij}}], \tag{18}$$

where $\mathbf{e_{ij}}$ is an unit vector perpendicular to the position vectors $\mathbf{C_{si}}$ and $\mathbf{C_{rj}}$, i.e.,

$$\mathbf{e_{ij}} = \frac{\mathbf{C_{si}} \times \mathbf{C_{rj}}}{R^2 \sin \phi_{ij}} \tag{19}$$

where $\mathbf{C_{si}} \times \mathbf{C_{rj}}$ denotes the vector cross-product of $\mathbf{C_{si}}$ and $\mathbf{C_{rj}}$. Thus, Equation (18), along with Equations (2) and (19) and a permeance model given by Equation (14), defines the torque generated by the spherical motor for a given set of inputs in terms of the magneto-motive-forces (mmf's) of the coils.

3. CONTROL INPUT OPTIMIZATION

The motion control of the VR spherical motor consists of two parts. The first part is to determine the actuating torques of the VR spherical motor so that the motor follows the desired trajectory. The second part determines the optimal electrical inputs to generate the required actuating torque determined by using the control law for tracking the desired trajectory. The computed torque method commonly used in the robot control is used in the first part of the control strategy. The control input optimization is addressed as follows.

The control input optimization is essentially an inverse problem to torque prediction model. The solution to the inverse problem is to compute a set of coil excitations, which is denoted here as a control input vector **U**, that is required to generate the desired torque. Unlike the forward torque prediction model which yields an unique torque vector for a specified set of coil excitations, there are generally infinite solutions to the inverse problem of the torque prediction model of a spherical VR motor for a specified torque. For clarity in illustrating the inverse torque model, the following additional assumptions are made: (1) Only current sources are used and the mmf's of the coil are treated as system input variables. (2) In practice, it is desired to have no wiring in the moving parts and thus, only simple iron cores with no excitation coils are assumed as rotor poles (i.e. $M_{rj} = 0$, j = 1 ,..., n).

3.1 Formulation for Inverse Torque Model

In order to obtain an optimal solution to the inverse torque model, the torque equation is presented in quadratic form using the following notations:

$$\mathbf{U} = [M_{s1} \ldots M_{sm}] \in R^m, \tag{20}$$

$$\mathbf{a} = [a_1 \ldots a_i \ldots a_m]^T, \tag{21}$$

and

$$a_i = \frac{\sum_{j=1}^{n} P_{ij}}{\sum_{i=1}^{m} \sum_{j=1}^{n} P_{ij}}, \qquad \sum_{i=1}^{m} a_i = 1 \tag{22}$$

i.e. except the i^{th} element which is equal to 1, all other elements of $\mathbf{c_i}$ are equal to 0. Hence, using the notations defined by Equations (20) to (22), the torque can be written in matrix form as follows:

$$\mathbf{T}_I = \frac{1}{2} \mathbf{U}^T [\mathbf{A}_I] \mathbf{U} \qquad I = 1, 2\ 3 \tag{23}$$

where

$$[\mathbf{A}_I] = \sum_{i=1}^{m} \left\{ \sum_{j=1}^{n} \left.\frac{dP(\phi)}{d\phi}\right|_{\phi=\phi_{ij}} (\mathbf{e_{ij}} \bullet \underline{\mathbf{u}}_I) \right\} (\mathbf{a} - \mathbf{c_i})(\mathbf{a} - \mathbf{c_i})^T \tag{24}$$

and $\underline{\mathbf{C}}_i = [0\ 0 \ldots 0\ \underset{i^{th}}{1}\ 0 \ldots 0\ 0]$

where ($\mathbf{u}_I$, I=1,2,3) is an unit vector along the axes of the rotor body frame. The matrices ($[\mathbf{A}_I]$, I=1,2,3) vary with the orientation of the spherical motor.

Given the desired torque, **U** may be determined from Equation (23) by solving the algebraic equations. However, since $\mathbf{U} \in R^m$ where m is the number of stator coils and is designed larger than three, there are generally infinite numbers of solutions to the inverse problem. The generalized reduced gradient (GRG) method [10] [11] is used to solve for the optimal input vector **U**, which minimizes the following cost function:

$$f(\mathbf{U}) = \sum_{i=1}^{m} |u_i|^p + M \sum_{I=1}^{3} (\tfrac{1}{2} \mathbf{U}^T [\mathbf{A}_I] \mathbf{U} - T_I)^2 \tag{25}$$

where the weighting factor M > 0 is generally a factor very large real number. The first term in the cost function is due to the current amplitude or the consumed electrical power, and the second term is a penalty term which takes into account the system constraint represented by Equation (23). Typical values of p are 1 and 2. When p is chosen as 1, the sum of the current amplitude is minimized. If the consumed power of the electrical circuit is to be minimized, p is set to be 2. The minimization of the cost function (25) is an unconstrained problem. It has been numerically found that the GRG method works well in minimizing the functional represented by Equation (25).

3.2 Illustrative Example

An example is illustrated here by using a design configuration where the stator and the rotor are arranged at the vertices of an icosahedron and a tetrahedron, respectively. The coordinates of four vertices of a tetrahedron for an unit sphere are described in TABLE 1. Similarly, the twelve coordinates describing the vertices of an unit icosahedron are listed in TABLE 2. However, to allow for the motion of the rotor shaft, only eleven stator poles are used in the design and pole 0 is irrelevant.

The characteristic dimensions of the VR spherical motor using in the following example are summarized as follows: The mean radius of the spherical surface separating the stator and the rotor pole faces are 38.1mm. The radius of the stator and the rotor poles is 12.7mm and the airgap separating the stator and the rotor pole faces is 1mm. The permeance model as a function of the relative displacement between two circular poles was obtained

experimentally. The value x_0 in Equation (13) was determined to be 18mm. With the permeance model and the given pole coordinates, the matrices ($\mathbf{A_I}$, I = 1, 2, and 3) are formed. To compute for an optimal input mmf's for a specified torque at a given orientation, an initial input mmf's vector is estimated and a local optimal solution is computed by the GRG algorithm. The global optimal solution is then searched by comparing the objective values of local optimal solutions.

Table 1 Coordinate of the stator poles

pole	x	y	z
0	0.0000	0.0000	0.0000
1	0.8944	0.0000	0.4472
2	0.2764	0.8507	0.4472
3	-0.7236	0.5257	0.4472
4	-0.7236	-0.5257	0.4472
5	0.2764	-0.8507	0.4472
6	-0.8944	0.0000	-0.4472
7	-0.2764	-0.8507	-0.4472
8	0.7236	-0.5257	-0.4472
9	0.7236	0.5257	-0.4472
10	-0.2764	0.8507	-0.4472
11	0.0000	0.0000	-1.0000

Table 2 Coordinates of the rotor poles

pole	x	y	z
1	0.9428	0.0000	0.3333
2	-0.4714	0.8165	0.3333
3	-0.4714	-0.8165	0.3333
4	0.0000	0.0000	-1.0000

As a numerical example, the optimal input mmf's which generate the torque $\mathbf{T} = 1\ \mathbf{u_3}$ (N-m) at the rotor orientation at (0,0,0) are computed for two cases. In both cases, p is set to be 2 so that the electric power is minimized and by choosing $M = 10^8$ the constraint equations are satisfied with the relative accuracy of 10^{-5}. In case (1), all the eleven input mmf's are independently excited. The values of the optimal input vector is tabulated in TABLE 3. The minimized objective value is 17.8601 and that the absolute value of the maximum input mmf is 3.7816×10^3 Amp-turns.

Table 3

pole	case 1 (10^3Amp-turns)	case 2 (10^3Amp-turns)
1	1.5797	0.3167
2	0.2390	-3.5868
3	-1.4074	0.6440
4	-0.4429	-3.8087
5	-3.7816	3.6894
6	1.1861	-0.3167
7	-1.5810	3.6894
8	0.1923	-0.6440
9	-0.2322	3.8087
10	3.4789	-3.6894
11	0.7682	3.0930
Objective Value	17.8601	46.2815

In case (2), the coil excitations are grouped in pairs so that the number of power amplifiers are reduced. In each grouping, the coils pointing towards each other along a diameter are connected in series, i.e. $u_i = -u_{i+5}$, i = 1, 2,.., 5. The optimal solution of case (2) is compared to that of case (1) in TABLE 3. The corresponding objective value is 46.2825 and the absolute value of the maximum mmf is 3.8087×10^3 Amp-turns. Clearly, the additional constraints introduced in case (2) substantially increase the objective value as compared to that in case (1).

It is worth noting that the input mmf's can be effectively lowered by reducing the airgap. If the airgap is reduced to 0.01mm, the current amplitudes for the same coils are about 1/10 of the the about results.

4. IMPLEMENTATION OF INVERSE MODEL

The average time to compute an optimal input vector using an off-the-shelf GRG optimization software [12] [13] is about 1 minute on an Intel 80386 25 MHz personal computer. For real time applications where the computation time is in the order of 1 msec, a look-up table must be pre-compiled off-line. The on-line look-up table should allow the pre-computed optimal input vector to be determined for a required torque at any given rotor orientations. If each of the six parameters (three torque components and three Euler angles) is characterized by N points over its operating range and two bytes are used to represent each of the n control inputs and the six parameters, the memory size required by the on-line look-up table will be $2nN^6$. For a system with 11 independently controlled inputs, the required memory size is over 1300 MBytes even if only 20 points are used to characterize each of the parameters. Two approaches, namely, parameter elimination and use of symmetry, are discussed in the following to reduce the table size required for practical implementation.

4.1 Table Size Reduction by Parameter Elimination

This approach is to eliminate the three torque parameters by introducing three control input vectors $\mathbf{U_1}$, $\mathbf{U_2}$, and $\mathbf{U_3}$ such that these control vectors would generate the unit torques $\mathbf{T}=(1,0,0)$, $\mathbf{T}=(0,1,0)$ and $\mathbf{T}=(0,0,1)$ about the three independent rotor axes respectively. For a specified torque at any arbitrary direction, the input vector $\mathbf{U}$ is then computed from Equation (26):

$$\mathbf{U} = \alpha\ \mathbf{U}_1 + \beta\ \mathbf{U}_2 + \gamma\ \mathbf{U}_3 . \qquad (26)$$

where α, β, and γ are constant coefficients to be determined for a specified torque. By substituting Equation (26) into Equation (23), we have

$$\frac{1}{2}\,[\alpha\ \beta\ \gamma]\,[\mathbf{B}_I]\begin{bmatrix}\alpha\\ \beta\\ \gamma\end{bmatrix} = \mathbf{T}_I , \qquad I = 1, 2, 3 , \qquad (27)$$

where

$$[\mathbf{B}_1] = \begin{bmatrix} 2 & \mathbf{U}_1^T\mathbf{A}_1\mathbf{U}_2 & \mathbf{U}_1^T\mathbf{A}_1\mathbf{U}_3 \\ \mathbf{U}_2^T\mathbf{A}_1\mathbf{U}_1 & 0 & \mathbf{U}_2^T\mathbf{A}_1\mathbf{U}_3 \\ \mathbf{U}_3^T\mathbf{A}_2\mathbf{U}_1 & \mathbf{U}_3^T\mathbf{A}_2\mathbf{U}_2 & 0 \end{bmatrix} ,$$

$$[\mathbf{B}_2] = \begin{bmatrix} 0 & \mathbf{U}_1^T\mathbf{A}_2\mathbf{U}_2 & \mathbf{U}_1^T\mathbf{A}_2\mathbf{U}_3 \\ \mathbf{U}_2^T\mathbf{A}_2\mathbf{U}_1 & 2 & \mathbf{U}_2^T\mathbf{A}_2\mathbf{U}_3 \\ \mathbf{U}_3^T\mathbf{A}_2\mathbf{U}_1 & \mathbf{U}_3^T\mathbf{A}_2\mathbf{U}_2 & 0 \end{bmatrix} ,$$

$$[\mathbf{B}_3] = \begin{bmatrix} 0 & \mathbf{U}_1^T\mathbf{A}_3\mathbf{U}_2 & \mathbf{U}_1^T\mathbf{A}_3\mathbf{U}_3 \\ \mathbf{U}_2^T\mathbf{A}_3\mathbf{U}_1 & 0 & \mathbf{U}_2^T\mathbf{A}_3\mathbf{U}_3 \\ \mathbf{U}_3^T\mathbf{A}_3\mathbf{U}_1 & \mathbf{U}_3^T\mathbf{A}_3\mathbf{U}_2 & 2 \end{bmatrix} .$$

The coefficients (α, β, γ) are computed from a set of three nonlinear simultaneous equations (27) and thus the required control input vector $\mathbf{U}$ can be solved from Equation (26). By storing the three input vectors $\mathbf{U_1}$, $\mathbf{U_2}$, and $\mathbf{U_3}$ for a given orientation in the precompiled table, the torque variables are eliminated and the memory size required in the look-up table is $6nN^3$ bytes.

It is worth noting that the need to compute the coefficients (α, β, γ) from a set of three non-linear simultaneous equations can

be eliminated if six additional constraints are imposed as follows:

$$\mathbf{U}_K\ [\mathbf{A}_J]\ \mathbf{U}_I = 0 \qquad (28)$$

for I, K $\neq$ J where I, J, K, = 1, 2, 3

which make all cross terms of $[\mathbf{B}_I]$ equal to zero. Therefore, without solving for (α, β, γ), **U** can be directly written as

$$\mathbf{U} = \sum_{I=1}^{3} \sqrt{T_I}\ \mathbf{U}_I \qquad (29)$$

4.2 Table Size Reduction by Use of Symmetry

Since the torque parameters are eliminated from the table, the control inputs are tabulated in terms of the rotor orientation only. Further reduction of the look-up table can be achieved by using the symmetry of the pole location to reduce the range of orientation parameters. A scheme was devised to illustrate the principle using a particular configuration where the stator and the rotor poles are arranged at the vertices of icosahedron and tetrahedron respectively. It is expected that similar arguments can be readily extended to other configurations where poles are arranged in the pattern of regular polygons.

The operating ZYZ Eulerian angles are $0 \le \psi \le 2\pi$, $|\theta| \le \pi/4$, and $0 \le \phi \le 2\pi$, where ψ, θ, ϕ are the precession, nutation, and spin angles respectively. If the resolution of the range of the parameters is r points/radian, the memory size of $2n(r\pi)^3$ bytes would be required if two bytes are used to represent a real number.

The rotor has four evenly spaced poles arranged at the apices of a tetrahedron. The position vectors of the rotor poles for an unit sphere are listed in TABLE 1. As shown in Fig. 4, since the three rotor poles, j =1,2,3, are evenly spaced at $2\pi/3$ radians apart at a plane perpendicular to the axis of the fourth pole (indicated as b in Fig. 4), an input vector $\mathbf{U}(\phi)$ would generate the same torque about the z-axis of the rotor as that would be generated by $\mathbf{U}(\phi \pm 2\pi/3)$ for any particular (ψ,θ). In other words, $\mathbf{U}(\phi \pm 2\pi/3) = \mathbf{U}(\phi)$ for a specified torque to spin the rotor about its z-axis. Thus, the range of the spin angle required in the formation of the look-up table is $0 \le \phi \le 2\pi/3$.

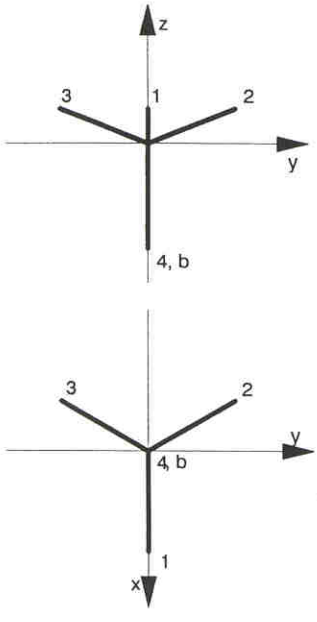

Fig. 4 Rotor Pole Configuration

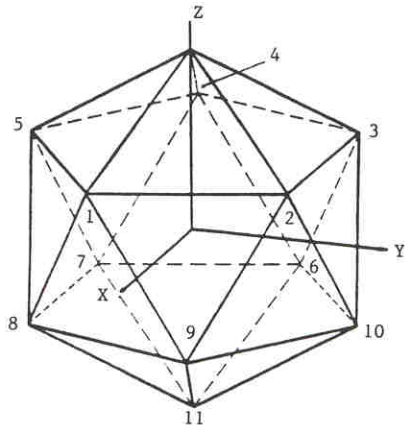

Fig. 5 Locations of Stator Poles

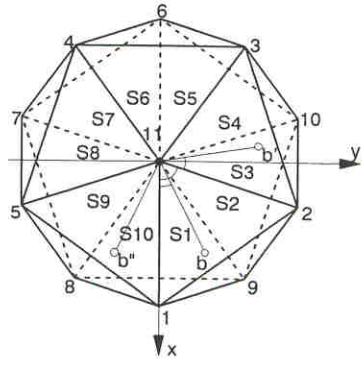

Fig. 6 Projection of Stator Pole on X-Y Plane

Fig. 5 shows the location of the eleven stator poles located at the apices of an icosahedron of unit radius. The position vectors of the stator poles are listed in TABLE 2, which are evenly spaced at $2\pi/5$ radians apart in two circular planes perpendicular to the axis of the eleventh pole. Fig. 6 shows the line projections of the stator pole axes on the xy plane. The space bounded between two adjacent projections is denoted as S_k (k = 1, ..., 10) in Fig. 6, where b is the projection of the end-point of the 4^{th} rotor pole on the xy plane.

Define the notation $\mathbf{U}^{(k)}$ to be an input vector **U** required to generate **T** when b $\in S_k$. The range of the precession angle required in the table formulation is such that b $\in S_1$. When b is outside the region S_1, the input vector $\mathbf{U}^{(k)}$ to generate the desired torque **T** can be deduced from the tabulated input vector $\mathbf{U}^{(1)}$ for the same torque by means of the transformation:

$$\mathbf{U}^{(k)} = \left[\begin{array}{cc|c} [R_k] & [0] & \begin{matrix}0\\ \vdots\\ 0\end{matrix} \\ [0] & [R_k] & \\ \hline 0\ \ 0\ \ldots\ 0\ \ 0 & & 1 \end{array}\right] \mathbf{U}^{(1)} \qquad (30)$$

The determination of the transformation $[\mathbf{R}_k]$ is separated into two cases; namely, an odd and an even number of k.

k is odd

Let (ψ, θ) denotes the position of b when b $\in S_1$. The corresponding position of b in S_3 is indicated as b′ in Fig. 5, which

can be written as $[\psi + (2\pi/5), \theta]$. To generate a desired torque when the position of the fourth pole is at $b' \in S_3$ using the lookup table, the input vector $\mathbf{U}^{(1)}$ is determined from the lookup table for the same desired torque at b and the input vector $\mathbf{U}^{(3)}$ is then obtained by shifting the index of the stator coils of the input vector $\mathbf{U}^{(1)}$ in the counter-clockwise direction, or equivalently by means of the transformation $[\mathbf{R_3}] = [\mathbf{R}]$ defined as follows:

$$[\mathbf{R}] = \begin{bmatrix} 0 & 0 & 0 & 0 & 1 \\ 1 & 0 & 0 & 0 & 0 \\ 0 & 1 & 0 & 0 & 0 \\ 0 & 0 & 1 & 0 & 0 \\ 0 & 0 & 0 & 1 & 0 \end{bmatrix} \tag{31}$$

In general, for any positions of $b \in S_k$ defined by $[\psi + (2\pi/5)k, \theta]$, the input vector $\mathbf{U}^{(k)}$ to generate the desired torque $\mathbf{T}$ can be deduced from $\mathbf{U}^{(1)}$ for the same torque using the Equation (28) where the transformation $[\mathbf{R_k}]$ is given by

$$[\mathbf{R_k}] = [\mathbf{R}]^{(k-1)/2} \tag{32}$$

k is even

Similarly, the input vector $\mathbf{U}^{(k)}$ required to generate the desired torque $\mathbf{T}$ when $b \in S_k$ (k is even) can be deduced from $\mathbf{U}^{(10)}$ for the same torque by means of Equations (28) and (29) or

$$\mathbf{U}^{(k)} = [\mathbf{R}]^{k/2}\ \mathbf{U}^{(10)}. \tag{33}$$

However, for any point b with its position denoted by $(\psi, \theta, \phi) \in S_1$, the point b" is a mirror image of b about the x-z plane. The position of b" can be written as $(-\psi, \theta, -\phi)$ or $(2\pi-\psi, \theta, 2\pi-\phi) \in S_{10}$. Since the symmetry between S_1 and S_{10} is mirror-like, the mirror image of the required torque when the position of the fourth pole is at $b'' \in S_{10}$ can be generated in terms of the input vector $\mathbf{U}^{(1)}$ when the position of the fourth pole is at $b \in S_1$. The mirror image of the torque can be produced by the input vector $\mathbf{U}^{(10)} = [\mathbf{R}_{10}]\ \mathbf{U}^{(1)}$ where transformation $[\mathbf{R}_{10}] = [\mathbf{R'}]$ is defined as follows:

$$[\mathbf{R'}] = \begin{bmatrix} 1 & 0 & 0 & 0 & 0 \\ 0 & 0 & 0 & 0 & 1 \\ 0 & 0 & 0 & 1 & 0 \\ 0 & 0 & 1 & 0 & 0 \\ 0 & 1 & 0 & 0 & 0 \end{bmatrix} \tag{34}$$

Denote the mirror image of the required torque $\mathbf{T}$ (when $b'' \in S_{10}$) as $\mathbf{T_e}$ (when $b \in S_1$) which is given by

$$\mathbf{T}_e = \begin{bmatrix} -1 & 0 & 0 \\ 0 & 1 & 0 \\ 0 & 0 & -1 \end{bmatrix} \mathbf{T}. \tag{35}$$

In general, for an even number of k,

$$[\mathbf{R_k}] = [\mathbf{R}]^{k/2}\ [\mathbf{R'}]\ . \tag{36}$$

The ranges of the Eulerian angles required in the formation of the table are reduced to

precession:	$0 \le \psi \le \pi/5$,
mutation:	$0 \le \theta \le \pi/4$, and
spin:	$0 \le \phi \le 2\pi/3$.

For the icosahedron/tetrahedron configuration, the required memory size is $n(r\pi)^3/15$ bytes, which represents 1/30 as the original range. It is expected that the memory size required by the table can be reduced to the order of 100 Kbytes.

5. CONCLUSIONS

The dynamic model and the control strategy of a three degrees-of-freedom VR spherical motor have been given in this paper. The dynamic model of the VR spherical motor consists of the rotor dynamics and the torque prediction. The torque prediction model has been derived as a function of the electromagnetic coil excitations and a permeance model as a function of the relative position between the rotor and the stator.

The inverse model of a VR spherical motor, which determines the coil excitations for a specified torque, is characterized by its infinite solutions. It has been shown in this paper that for a current controlled spherical motor, the relationship between the output torque and the input currents are algebraic and quadratic. The torque prediction model of a current controlled VR spherical motor is decoupled from the dynamic equations of the system, and therefore allows the determination of the optimal electrical inputs to be separated from the motion control of the spherical rotor.

Along with the formulation of input vector optimization, the method of designing a lookup table for the practical implementation of the optimal solution in real-time has also been discussed in this paper. It has been shown that the memory size of the lookup table can be effectively reduced by parameter elimination and by making use of the symmetry property of the pole configuration.

Acknowledgements This work is supported by the National Science Foundation under grant numbers DMC 8810146 and DDM-8958383.

REFERENCES

1. Vachtsevanos, G.J., and Davey K., and Lee, K.-M. "Development of a Novel Intelligent Robotic Manipulator," IEEE Control Systems Magazine, June 1987.
2. Devay, K. and Vachtsevanos, G. "The Analysis of Fields and Torques in a Spherical Induction motor," IEEE Trans. Magnetics, Vol. MAG-23, March 1987.
3. Lee, K.-M., Vachtsevanos, G. and Kwan C-K., " Development of a Spherical Stepper Wrist Motor," Proceedings of the 1988 IEEE International Robotics and Automation. Philadelphia, April 25-29, 1988.
4. Hollis, R. L., Allan, A.P. and Salcudan, S., "A Six Degree-of-Freedom Magnetically Levitated Variable Compliance Fine Motion Wrist," Proceedings of the fourth International Symposium on Robotics Research, Santa Cruz, August 1987.
5. Kaneko, K., Yamada, I., and Itao, K., "A Spherical DC Servo Motor with Three Degrees-of-Freedom," ASME Trans. on Dynamic Systems, Measurement and Control, Vol. III, November 3, September 1989, pp. 398-402.
6. Foggia, A., Oliver, E., Chappnis, F. and Sabonnadiere, J., "New Three Degree of Freedom Electromagnetic Actuator," Conference Record - IAS Annual Meeting, Vol. 35, No. 6, Published by IEEE, New York, NY, USA; 1988, pp. 137-141.
7. Lee, K.-M. and Kwan C-K., " Design Concept Development of a Spherical Stepper Wrist Motor," IEEE Journal of Robotics and Automation, Vol. 7, No. 1, Feb. 1991, pp. 175-181.
8. Smith, D. E., "Essentials of Plane and Solid Geometry," Wentworth-Smith Mathematical Series, 1923
9. Lee K.-M. and Pei, J. "Kinematic Analysis of a Three Degrees-of-Freedom Spherical Wrist Actuator," Proceedings of the fifth International Conference on Advanced Robotics, Pisa, Italy. June 20-22, 1991.
10. Wolfe, P., "Methods for Linear Constraints," Nonlinear Programming, North Holland, 1967.
11. Wolfe, P., "Methods of Nonlinear Programming," Recent Advances in Mathematical Programming, McGraw-Hill, New York, 1968.
12. Abadie, J. and Carpentier, J., "Generalization of the Wolfe Reduced Gradient Method to Case of Nonlinear Constraints," Optimization, Academic Press, 1969.
13. Lasdon, L.S., and Warren, A.D., "GRG2 User's Guide," University of Texas at Austin, 1989.